IEEE Photonics Journal
An IEEE Photonics Society Publication

Open Access

Chip-Scale Plasmonic Sum Frequency Generation

Volume 9, Number 3, June 2017

Songang Bai
Ming Fang
Wei E. I. Sha
Yurui Qu
Zhongwei Jin
Jingyi Tian
Kaikai Du
Shaoliang Yu
Cheng-Wei Qiu
Min Qiu
Qiang Li

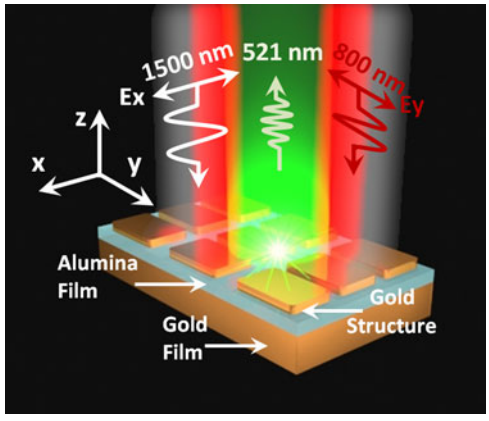

DOI: 10.1109/JPHOT.2017.2705061
1943-0655

IEEE photonics SOCIETY

IEEE

Chip-Scale Plasmonic Sum Frequency Generation

Songang Bai,[1] Ming Fang,[2,3] Wei E. I. Sha,[3] Yurui Qu,[1] Zhongwei Jin,[4] Jingyi Tian,[1] Kaikai Du,[1] Shaoliang Yu,[1] Cheng-Wei Qiu,[4] Min Qiu,[1] and Qiang Li[1]

[1]State Key Laboratory of Modern Optical Instrumentation, College of Optical Science and Engineering, Zhejiang University, Hangzhou 310027, China
[2]Key Laboratory of Intelligent Computing and Signal Processing, Ministry of Education, Anhui University, Hefei 230039, China
[3]Department of Electrical and Electronic Engineering, The University of Hong Kong, Pokfulam, Hong Kong
[4]Department of Electrical and Computer Engineering, National University of Singapore, 117583 Singapore

DOI:10.1109/JPHOT.2017.2705061

Manuscript received April 22, 2017; revised May 12, 2017; accepted May 13, 2017. Date of publication June 1, 2017; date of current version June 8, 2017. This work was supported in part by the National Key Research and Development Program of China (No. 2017YFA0205700) and the National Natural Science Foundation of China under Grants 61235007, 61425023, and 61575177. This paper has supplementary downloadable material available at http://ieeexplore.ieee.org (File size: 174 KB). Corresponding authors: Wei E. I. Sha and Qiang Li (e-mail: wsha@eee.hku.hk; qiangli@zju.edu.cn).

Abstract: Plasmonics provides a promising candidate for nonlinear optical interactions because of its ability to enable extreme light concentration at the nanoscale. We demonstrate on-chip plasmonic sum frequency generation (SFG) with a metal—dielectric–metal nanostructure. The two cross-polarized pumps (800 and 1500 nm) are designed to match the two resonances of this plasmonic nanostructure to make the most of the electric field enhancement and spatial overlapping of the modes. Since these two resonances are predominantly determined by the sizes of the top metallic nanostructures in the same direction, the SFG (521 nm) can be independently controlled by each pump via changing these sizes. This study exerts the full strength of plasmonic resonance induced field enhancement, thereby paving a way toward using nanoplasmonics for future nonlinear nanophotonics applications, such as optical information processing, imaging, and spectroscopy.

Index Terms: Plasmonics, metamaterials and nonlinear optics.

1. Introduction

Nowadays metal nanostructures have been widely used in many areas such as super-resolution imaging [1], [2], information processing [3], [4] and molecular detection [5], [6] due to their strong local electric field enhancement by surface plasmon polaritions (SPPs). This electric field enhancement can be further boosted by resonances and advantageously exploited for amplifying nonlinear effects [7]–[13]. Besides, the requirement for phase matching, which is conventionally of vital necessity for the nonlinear effect, has been eliminated since the sizes of the metal nanostructures are much smaller than the wavelength of light. Based on the resonant plasmonic nanostructures, a multitude of nonlinear processes have been explored, including second-harmonic generation

(SHG) [14]–[20], third-harmonic generation (THG) [21]–[25], four-wave mixing [26]–[30], difference-frequency generation [31] and sum-frequency generation (SFG) [32], [33].

In particular, SFG has attracted significant attention owing to its surface-sensitive and high-controllable capability for the new frequency generation. In the SFG, two different photons merge into a new photon at the frequency of the sum of these two photons (ω_1, $\omega_2 \rightarrow \omega_1 + \omega_2$). The SFG at the nanoscale has been employed in the molecular detection/imaging with sum-frequency generation vibrational spectroscopy (SFG-VS) or near-field scanning optical microscopy [34]–[40], where the SFG is maximized by tailoring one of the pump frequency to match the vibrational frequency of molecules residing at surfaces (such as Al_2O_3 surfaces [41], [42], gold nanoparticle or gold film surfaces [43]–[45], $BaTiO_3$-core gold-shell nanoparticle surfaces [46]). It is important to note that, in aforementioned SFG configurations, the main topics are focused on the detection of the molecules, not the enhancement of the SFG signal for nonlinear signal processing. Alternatively, in view of a pronounced field enhancement and multiple designs, plasmonic resonance could offer a new avenue for SFG in chip-scale integration and applications. Also the SFG from plasmonic nanostructures is observed in [32], [33], but these papers are explicitly focused on SHG or THG while the SFG is only simply mentioned.

In this paper, a resonant metal-dielectric-metal (MIM) plasmonic nanostructure with electric field enhancement is adopted to generate the SFG signal. The plasmonic MIM nanostructure is designed and fabricated to possess two lattice directions with engineered sizes along those two directions, such that two plasmon resonances can be excited independently by two orthogonal polarized pump lasers with two corresponding pump wavelengths. This SFG in the resonant MIM plasmonic nanostructure exhibits several distinctive advantages. (i) The SFG can be significantly amplified by the electric field enhancement in the MIM plasmonic nanostructure. (ii) The two pump wavelengths of SFG can be independently tuned through geometric design and precise fabrication of the metal pattern in the MIM nanostructure. (iii) With subwavelength feature size, ultrathin and flat profile, this plasmonic SFG is promising for chip-scale integration and applications.

2. Experiment and Discussion

A MIM nanostructure (see Fig. 1(a)) with well-designed resonances is utilized to realize the SFG at the nanoscale. This MIM nanostructure is composed of three layers: a 100-nm-thick gold slab at the bottom to prevent the back leak of the confined field, 30-nm-thick rectangular periodic gold nanostructures (with an extra 5-nm-thick Cr adhesion layer) at the top and a 14-nm-thick alumina film in between, while the substrate is glass, which doesn't influence the resonances. For this MIM resonator, the electromagnetic fields are strongly confined in the middle dielectric layer at resonances [47]–[51]. The total thickness of the MIM nanostructure is only 150 nm. The periods of the MIM nanostructure are 200 nm and 350 nm in the x- and y- directions, respectively, which are smaller than the light wavelength. The scanning electron microscope image (see Fig. 1(b)) of the fabricated MIM nanostructure demonstrates the uniformity of the top gold nanostructures. The wavelengths of the two cross-polarized pumps for SFG are matched to the two cross-polarized resonances of the nanostructure, so as to excite and fully utilize the plasmon-induced field enhancement. The resonant wavelength for a specific polarization direction is predominantly determined by the length of the top nanostructures along the corresponding direction, thereby providing an avenue for independent control over the two cross-polarized pumps. The lengths of the top nanoparticles are 160 nm and 250 nm in the x- and y- directions, respectively. This design guarantees one resonance at 1500 nm for the x-polarized pump and the other at 800 nm for the y-polarized pump. The fabrication of the MIM nanostructure and SFG experiment method are shown in the Supplementary Information.

The measured linear reflection spectra of the MIM nanostructure from 500 to 1700 nm wavelength for both the x- and y-polarized light are shown in Fig. 1(c). These two resonant wavelengths (1500 nm and 800 nm) are adopted as the wavelengths of Pump X and Pump Y. In the SFG experiment, these two pumps (110-fs pulses) are superposed and focused onto the MIM nanostructure (see Fig. 1(a)). Fig. 1(d) provides the spectra of the generated sum-frequency signal. Strong SFG signal around 521 nm can be observed, while no distinguishable signal can be recorded from the insulator-metal (IM) reference film (with only the middle dielectric layer and bottom gold film).

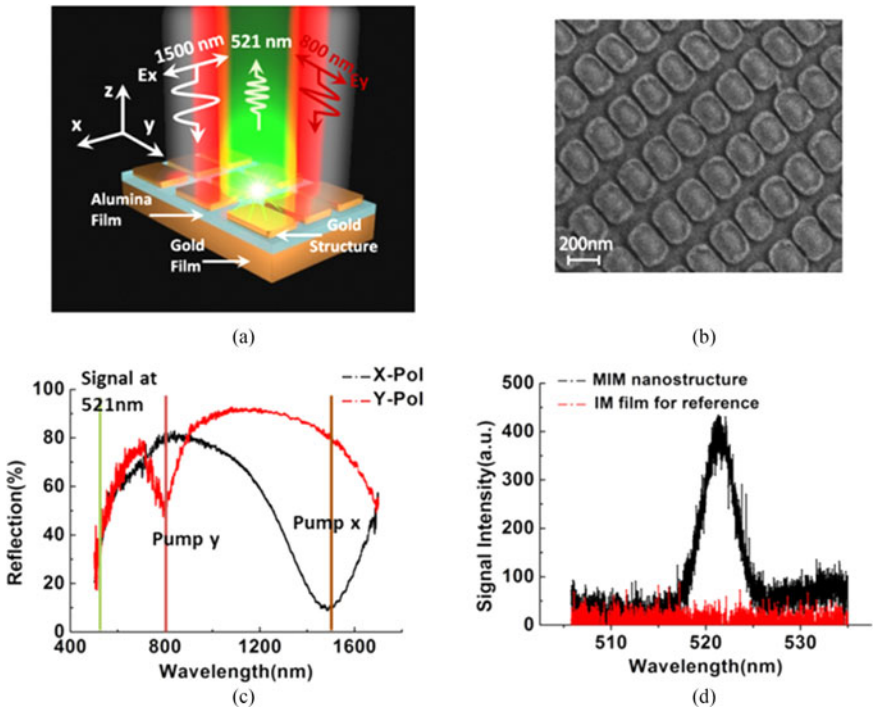

Fig. 1. (a) Schematic of the SFG experiment. The substrate is glass (not shown here). The two pump beams are polarized in the x- and y-direction. (b) The SEM image of the MIM nanostructure. (c) Measured linear reflections of the fabricated MIM nanostructure. X-pol and Y-pol denote the polarization of the incident light. The wavelengths of the two cross-polarized pump beams and the signal beam are indicated by The vertical lines. (d) Measured SFG signal for the MIM nanostructure and the IM film for reference.

Different incident powers, pump wavelengths and polarizations are attempted in various control experiments in order to probe the full characteristics of the SFG signal. The relation between the signal intensity and the incident power can be used to identify or evaluate the order of the nonlinear process. The SFG is a second-order parametric process [52] and the nonlinear polarization is proportional to the product of the electric field amplitudes of the two pumps. Correspondingly, the nonlinear signal intensity is proportional to the product of the two pump powers, i.e., (and denote the pump powers of 800 nm and 1500 nm lasers, respectively). Two situations with different pump powers are experimentally investigated in Fig. 2(a). In one case, the total pump power (also the incident power) is tuned from 10 mW to 70 mW while the power ratio is kept at 5:2. The experimental data are fitted to follow a straight line (black line in Fig. 2(a)) in log-scale plot (power law) with a slope of 1.99, undoubtedly verifying the quadratic correlation between the SFG intensity and the total pump power. In the other case, the 1500 nm pump power varies from 10 mW to 50 mW while the 800 nm pump power is maintained at 20 mW. A slope of 1.00 is obtained by fitting the data as shown in the brown line in Fig. 2(a), confirming the linear relation between the signal intensity and one pump power.

The SFG signal wavelength can also be tunable by changing the pump wavelength. The SFG signals with Pump X changing from 1470 nm to 1530 nm with an interval of 10 nm are reported in Fig. 2(b). Each SFG signal is normalized by the maximum of its SFG peak because the change of the pump wavelength affects the spatial overlap of the two pump pulses and the resultant SFG signal intensity. The wavelengths of the SFG can be continuously tuned from 518 nm to 525 nm with the wavelength of Pump X changing from 1470 nm to 1530 nm. The photoluminescence intensity turns weaker in comparison with the SFG signal intensity, as the SFG signal wavelength increases. The THG signal of Pump X at 1530 nm also shifts to the measured spectrum range, as indicated by the spike around 510 nm in the dark blue line in Fig. 2(b).

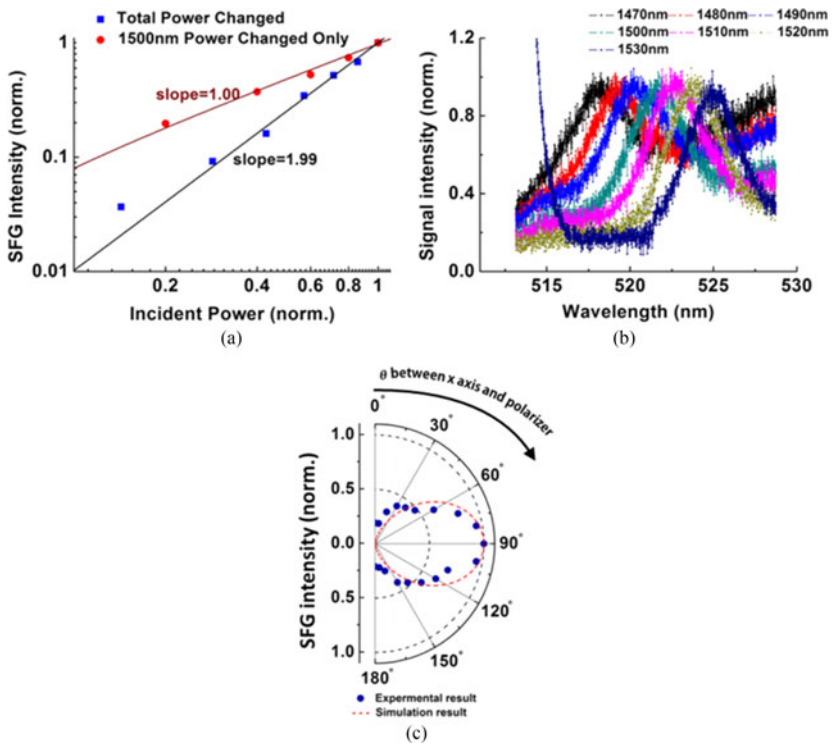

Fig. 2. (a) The SFG intensity at different incident powers. In the case of changing total power, the incident power is the total power (from 10 mW to 70 mW) of both pump beams while the power ratio is kept at I1500:I800 = 5:2. In the case of changing 1500 nm power, the incident powers the 1500 nm pump power (from 10 mW to 50 mW) while the 800 nm pump power is kept at 20 mW. (b) Measured SFG signal when the wavelength of Pump X changes from 1470 nm to 1530 nm with a step size of 10 nm. The spike in the dark blue line around 510 nm for the 1530 nm pump corresponds to the third-harmonic generation. (c) Measured and simulated SFG signal intensity at different polarizations. θ is the angle between the x axis and the polarizer before the spectrometer.

The polarization of the SFG is further explored by inserting a polarizer before the spectrometer in the measurement setup (see Fig. S1). The measured SFG signal intensity at different polarizations is illustrated in Fig. 2(c) by rotating the angle θ between the x axis and the polarizer in the case of equal excitation power for Pump X and Pump Y. The y-polarized component dominates in the SFG signal which agrees with the simulation result.

3. Simulation and Discussion

To unveil the physics governing this SFG from the MIM nanostructure, the Maxwell-hydrodynamic equations are adopted to model the SFG from the MIM nanostructures [53]–[56].

In this simulation, Maxwell-hydrodynamic equations are solved non-perturbatively and self-consistently by the finite-difference time-domain (FDTD) method with Yee grids. Using a pure scattered field technique, the governing equations including Maxwell, hydrodynamic and current continuity equations are shown below:

$$\nabla \times \mathbf{E}_{\text{sca}} = -\mu_0 \frac{\partial \mathbf{H}_{\text{sca}}}{\partial t}, \quad \nabla \times \mathbf{H}_{\text{sca}} = \mathbf{J} + \varepsilon_0 \frac{\partial \mathbf{E}_{\text{sca}}}{\partial t} \tag{1}$$

$$\frac{\partial \mathbf{v}}{\partial t} + \mathbf{v} \cdot \nabla \mathbf{v} + \gamma \mathbf{v} = \frac{-e}{m} (\mathbf{E}_{\text{inc}} + \mathbf{E}_{\text{sca}} + \mu_0 \mathbf{v} \times (\mathbf{H}_{\text{inc}} + \mathbf{H}_{\text{sca}})) + \nabla V_P \tag{2}$$

$$\frac{\partial n}{\partial t} = -\nabla \cdot (n\mathbf{v}), \quad \mathbf{J} = -en\mathbf{v} \tag{3}$$

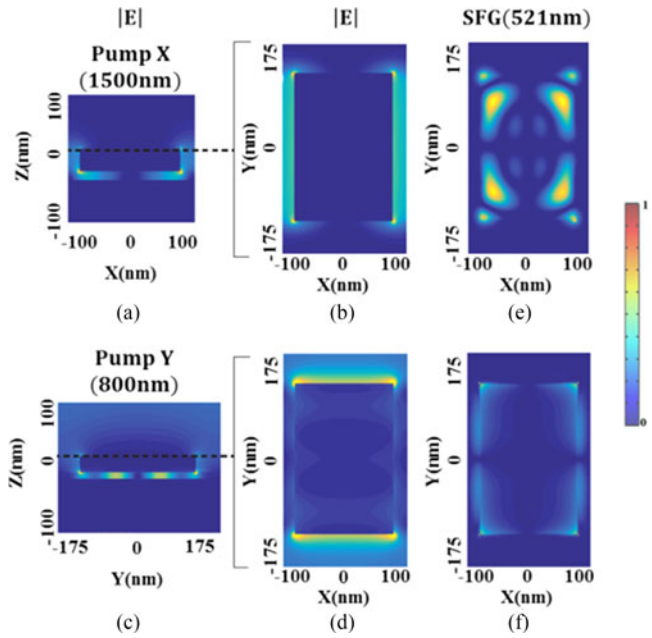

Fig. 3. (a)–(d) are calculated electric field amplitudes at Pump X and Pump Y wavelength, respectively. (a), (c), and (b), (d) correspond to XZ-cut-plane at y = 0, YZ-cut-plane at x = 0, XY-cut-plane in the middle of the metal layer, respectively. (e) and (f) are the calculated electric field amplitude at SFG wavelength (521 nm), corresponding to XY-cut-planes in the dielectric and metal layer, respectively. All the results are calculated by Maxwell-hydrodynamic model.

Where $\mathbf{E}_{sca}$ and $\mathbf{H}_{sca}$ are the scattered electric and magnetic fields produced by the polarization current $\mathbf{J}$. And $\mathbf{E}_{inc}$ and $\mathbf{H}_{inc}$ are the incident electric and magnetic fields produced by the pump laser. Moreover, $\mathbf{v}$ is the electron velocity and the convective acceleration term $\mathbf{v} \cdot \nabla \mathbf{v}$ is one of the key contributors to the sum frequency generation. Furthermore, γ is the scattering rate related to the metallic loss. The potential V_p including Hartree, exchange, Fermi and Bohm potentials can be incorporated to capture the nonlocal and quantum effects. These effects can be ignored for the nanostructures with a size typically larger than 10 nm. Additionally, e and m are the elementary charge and electron mass, and n is the electron density. Here, the current continuity equation Eq. (3) is used to connect Maxwell equation Eq. (1) and hydrodynamic equation Eq. (2). Equations (1)–(3) provide self-consistent formulations of free electron gas in a plasmonic system.

The parameters for gold are taken to be $n_0 = 5.91 \times 10^{28}$ m^{-3} and $\gamma = 9.46 \times 10^{12}$ s^{-1}. Nonlinearity of chromium is considered in the simulation, and the constants for chromium are taken to be $n_0 = 1.9002 \times 10^{29}$ m^{-3} and $\gamma = 2.534 \times 10^{14}$ s^{-1}. The Al_2O_3 layer is treated as a dielectric material without nonlinearity and its relative permittivity is 3.2. The incident plane wave is a cosine-modulated Gaussian pulse. The detailed numerical implementation of the Maxwell-hydrodynamic model has been presented in our previous works [55]. Through comparing to the boundary element method that only considers surface contribution [56], [57], we have confirmed that the Maxwell-hydrodynamic model is a nonperturbative description of free-electron nonlinearity allowing accounting for both bulk and surface contributions of the nonlinear generation process.

By using this method, the SFG signal under the two cross-polarized incidences is theoretically modeled. The electric field amplitudes at the SFG wavelength (521 nm) are depicted in Fig. 3(e), (f). The electric field pattern for the SFG resembles the product of the fundamental electric-fields from the two pumps (see Fig. 3(b) and (d)), concluding that the SFG originates from the spatial overlap of fundamental electric fields under the two cross-polarized pumps in the MIM nanostructure. The calculated polarization of the SFG signal shows that the electric field is predominantly polarized in the y-direction, in accordance with the experimental result (see Fig. 2(c)).

TABLE 1
The Surface and Bulk Contributions for the Sum Frequency Generation

	Integration of Polarization Current at the Sum Frequency	Bulk Contribution	Surface Contribution
Upper Au	$\sum$ **Jx**	**0.105**	**0.016**
	$\sum$ **Jy**	**1**	**0.0153**
Lower Au	$\sum$ **Jx**	**0.032**	**0.12e−5**
	$\sum$ **Jy**	**0.210**	**0.56e−5**

To figure out the surface and bulk contributions of the SFG, the net polarization currents of both the upper and lower gold nanostructures at the sum frequency are integrated separately for bulk and surface regions. The surface regions include the outmost Yee grids with a spatial size of 1 nm at the surface of the nanostructures. The bulk regions include all the Yee grids of the nanostructures excluding the outmost Yee grids. The results are summarized in Table 1, all the results are normalized by the maximum integration value i.e., $\sum J_y$ (at the bulk region of the upper gold nanostructure). One can see that the contribution from the lower gold nanostructure is weak than that from the upper gold nanostructure. Because the incident power from the two pumps are partially absorbed by the upper nanostructure. Most importantly, the sum frequency generation is due to the bulk polarization current along the y direction. Due to centrosymmetry at the xoy plane, the surface contributions from the two nanostructures are ignorable. The bulk contribution of sum-frequency generation is proportional to the spatial derivatives of electric-field; and the bulk contribution will increase if electric-field is significantly varying in the bulk of the metal. The high-order magnetic resonance induces a long-range light-matter interaction and significant electric-field gradient along the y direction, which produces the dominant nonlinear response.

4. Conclusion

In conclusion, based on the MIM plasmonic nanostructures, SFG is obtained with a strong resonance-induced field enhancement. To make full use of the electric field enhancement, the two cross-polarized pumps are designed to spectrally match the two resonance frequencies of the MIM nanostructure and meanwhile the two resonance modes are designed to be spatially overlapped with each other for producing a strong SFG signal. Since each resonance is predominantly determined by the size of the top film in the same direction, the SFG can be independently controlled by each pump. These results substantially broaden the scope of nonlinear generation in the resonant plasmonic nanostructures and represent a key step towards using nanoplasmonic for future nonlinear nanophotonics applications, such as optical information processing, imaging and spectroscopy.

Acknowledgment

The authors would like to thank the anonymous reviewers for their valuable suggestions.

References

[1] X. C. Zhou *et al.*, "Quantitative super-resolution imaging uncovers reactivity patterns on single nanocatalysts," *Nature Nanotechnol.*, vol. 7, no. 4, pp. 237–241, Apr. 2012.
[2] J. N. Anker, W. P. Hall, O. Lyandres, N. C. Shah, J. Zhao, and R. P. Van Duyne, "Biosensing with plasmonic nanosensors," *Nature Mater.*, vol. 7, no. 6, pp. 442–453, Jun. 2008.

[3] K. F. MacDonald, Z. L. Samson, M. I. Stockman, and M. I. Zheludev, "Ultrafast active plasmonics," *Nature Photon.*, vol. 7, no. 1, pp. 55–58, Jan. 2009.
[4] M. Wagner and M. Liu, "Plasmonics: An ultrafast plasmonic tuning knob," *Nature Photon.*, vol. 10, no. 4, pp. 210–211, Apr. 2016.
[5] P. Zijlstra, P. M. Paulo, and M. Orrit, "Optical detection of single non-absorbing molecules using the surface plasmon resonance of a gold nanorod," *Nature Nanotechnol.*, vol. 7, no. 6, pp. 379–382, Jun. 2012.
[6] S. J. Tan, M. J. Campolongo, D. Luo, and W. Cheng, "Building plasmonic nanostructures with DNA," *Nature Nanotechnol.*, vol. 6, no. 5, pp. 268–276, May 2011.
[7] C. Barsi and J. W. Fleischer, "Nonlinear Abbe theory," *Nature Photon.*, vol. 7, no. 8, pp. 639–643, Aug. 2013.
[8] J. Butet, I. Russier-Antoine, C. Jonin, N. Lascoux, E. Benichou, and P. F. Brevet, "Sensing with multipolar second harmonic generation from spherical metallic nanoparticles," *Nano Lett.*, vol. 12, no. 3, pp. 1697–1701, Mar. 2012.
[9] M. Kauranen and A. V. Zayats, "Nonlinear plasmonics," *Nature Photon.*, vol. 6, no. 11, pp. 737–748, Nov. 2012.
[10] G. Bautista, M. J. Huttunen, J. Mäkitalo, J. M. Kontio, J. Simonen, and M. Kauranen, "Second-harmonic generation imaging of metal nano-objects with cylindrical vector beams," *Nano Lett.*, vol. 12, no. 6, pp. 3207–3212, Jun. 2012.
[11] A. Stolz *et al.*, "Nonlinear photon-assisted tunneling transport in optical gap antennas," *Nano Lett.*, vol. 14, no. 5, pp. 2330–2338, May 2014.
[12] M. Mesch, B. Metzger, M. Hentschel, and H. Giessen, "Nonlinear plasmonic sensing," *Nano Lett.*, vol. 16, no. 5, pp. 3155–3159, May 2016.
[13] N. Segal, S. Keren-Zur, N. Hendler, and T. Ellenbogen, "Controlling light with metamaterial-based nonlinear photonic crystals," *Nature Photon.*, vol. 9, no. 3, pp. 180–184, Mar. 2015.
[14] M. Celebrano *et al.*, "Mode matching in multiresonant plasmonic nanoantennas for enhanced second harmonic generation," *Nature Nanotechnol.*, vol. 10, no. 5, pp. 412–417, May 2015.
[15] L. Black *et al.*, "Tailoring second-harmonic generation in single L-shaped plasmonic nanoantennas from the capacitive to conductive coupling regime," *ACS Photon.*, vol. 2, no. 11, pp. 1592–1601, Nov. 2015.
[16] J. Butet, P. F. Brevet, and O. J. Martin, "Optical second harmonic generation in plasmonic nanostructures: From fundamental principles to advanced applications," *ACS Nano*, vol. 9, no. 11, pp. 10545–10562, Nov. 2015.
[17] Y. Zhang, N. K. Grady, C. Ayala-Orozco, and N. J. Halas, "Three-dimensional nanostructures as highly efficient generators of second harmonic light," *Nano Lett.*, vol. 11, no. 12, pp. 5519–5523, Dec. 2011.
[18] K. Thyagarajan, J. Butet, and O. J. Martin, "Augmenting second harmonic generation using fano resonances in plasmonic systems," *Nano Lett.*, vol. 13, no. 4, pp. 1847–1851, Apr. 2013.
[19] S. D. Liu *et al.*, "Polarization-independent multiple fano resonances in plasmonic nonamers for multimode-matching enhanced multiband second-harmonic generation," *ACS Nano*, vol. 10, no. 1, pp. 1442–1453, Jan. 2016.
[20] J. Lee *et al.*, "Giant nonlinear response from plasmonic metasurfaces coupled to intersubband transitions," *Nature*, vol. 511, no. 7507, pp. 65–69, Jul. 2014.
[21] H. Aouani, M. Rahmani, M. Navarro-Cía, and S. A. Maier, "Third-harmonic-upconversion enhancement from a single semiconductor nanoparticle coupled to a plasmonic antenna," *Nature Nanotechnol.*, vol. 9, no. 14, pp. 290–294, Apr. 2014.
[22] G. Hajisalem, M. S. Nezami, and R. Gordon, "Probing the quantum tunneling limit of plasmonic enhancement by third harmonic generation," *Nano Lett.*, vol. 14, no. 11, pp. 6651–6654, Nov. 2014.
[23] M. R. Shcherbakov *et al.*, "Nonlinear interference and tailorable third-harmonic generation from dielectric oligomers," *ACS Photon.*, vol. 2, no. 5, pp. 578–582, May 2015.
[24] B. Metzger *et al.*, "Doubling the efficiency of third harmonic generation by positioning ITO nanocrystals into the hot-spot of plasmonic gap-antennas," *Nano Lett.*, vol. 14, no. 5, pp. 2867–2872, May 2014.
[25] B. Metzger, T. Schumacher, M. Hentschel, M. Lippitz, and H. Giessen, "Third harmonic mechanism in complex plasmonic fano structures," *ACS Photon.*, vol. 1, no. 6, pp. 471–476, Jun. 2014.
[26] S. Palomba, S. Zhang, Y. Park, G. Bartal, X. Yin, and X. Zhang, "Optical negative refraction by four-wave mixing in thin metallic nanostructures," *Nature Mater.*, vol. 11, no. 1, pp. 34–38, Jan. 2012.
[27] M. Danckwerts and L. Novotny, "Optical frequency mixing at coupled gold nanoparticles," *Phys. Rev. Lett.*, vol. 98, no. 2, p. 026104, Jan. 2007.
[28] H. Suchowski, K. O'Brien, Z. J. Wong, A. Salandrino, X. Yin, and X. Zhang, "Phase mismatch–free nonlinear propagation in optical zero-index materials," *Science*, vol. 342, no. 6163, pp. 1223–1226, Dec. 2013.
[29] Y. Zhang, F. Wen, Y. R. Zhen, P. Nordlander, and N. J. Halas, "Coherent fano resonances in a plasmonic nanocluster enhance optical four-wave mixing," *Proc. Nat. Acad. Sci.*, vol. 110, no. 23, pp. 9215–9219, Jun. 2013.
[30] Y. Jung, H. Chen, L. Tong, and J. X. Cheng, "Imaging gold nanorods by plasmon-resonance-enhanced four wave mixing," *J. Phys. Chem. C*, vol. 113, no. 7, pp. 2657–2663, Feb. 2009.
[31] Y. Zhang *et al.*, "Toward surface plasmon-enhanced optical parametric amplification (SPOPA) with engineered nanoparticles: A nanoscale tunable infrared source," *Nano Lett.*, vol. 16, no. 5, pp. 3373–3378, May 2016.
[32] S. Palomba, M. Danckwerts, and L. Novotny, "Nonlinear plasmonics with gold nanoparticle antennas," *J. Opt. A-Pure Appl. Opt.*, vol. 11, no. 11, p. 114030, Nov. 2009.
[33] G. Sartorello *et al.*, "Ultrafast optical modulation of second- and third-Harmonic generation from cut-disk-based metasurfac," *ACS Photon.*, vol. 3, no. 8, pp. 1517–1522, Aug. 2016.
[34] W. T. Liu and Y. R. Shen, "In situ sum-frequency vibrational spectroscopy of electrochemical interfaces with surface plasmon resonance," *Proc. Nat. Acad. Sci.*, vol. 111, no. 4, pp. 1293–1297, Jan. 2014.
[35] A. D. Quast, F. Zhang, M. R. Linford, and J. E. Patterson, "Back-surface gold mirrors for vibrationally resonant sum-frequency (VR-SFG) spectroscopy using 3-mercaptopropyltrimethoxysilane as an adhesion promoter," *Appl. Spectrosc.*, vol. 65, no. 6, pp. 634–641, Jun. 2011.
[36] R. D. Schaller, J. C. Johnson, K. R. Wilson, L. F. Lee, L. H. Haber, and R. J. Saykally, "Nonlinear chemical imaging nanomicroscopy: From second and third harmonic generation to multiplex (broad-bandwidth) sum frequency generation near-field scanning optical microscopy," *J. Phys. Chem. B*, vol. 106, no. 20, pp. 5143–5154, May 2002.

[37] Y. R. Shen and V. Ostroverkhov, "Sum-frequency vibrational spectroscopy on water interfaces: Polar orientation of water molecules at interfaces," *Chem. Rev.*, vol. 106, no. 4, pp. 1140–1154, Apr. 2006.
[38] A. G. de Beer, and S. Roke, "Nonlinear mie theory for second-harmonic and sum-frequency scattering," *Phys. Rev. B*, vol. 79, no. 15, p. 155420, Apr. 2009.
[39] G. Tourillon, L. Dreesen, C. Volcke, Y. Sartenaer, P. A Thiry, and A. Peremans, "Total internal reflection sum-frequency generation spectroscopy and dense gold nanoparticles monolayer: A route for probing adsorbed molecules," *Nanotechnology*, vol. 18, no. 41, Oct. 2007, Art. no. 415301.
[40] A. N. Bordenyuk *et al.*, "Vibrational sum frequency generation spectroscopy of dodecanethiol on metal nanoparticles," *J. Phys. Chem. B*, vol. 111, no. 25, pp. 8925–8933, Jun. 2007.
[41] H. A. Al-Abadleh and V. H. Grassian, "FT-IR study of water adsorption on aluminum oxide surfaces," *Langmuir*, vol. 19, no. 2, pp. 341–347, Jan. 2003.
[42] M. T. Casford and P. B. Davies, "The structure of oleamide films at the aluminum/oil interface and aluminum/air interface studied by sum frequency generation (SFG) vibrational spectroscopy and reflection absorption infrared spectroscopy (RAIRS)," *ACS Appl. Mater. Interf.*, vol. 1, no. 8, pp. 1672–1681, Aug. 2009.
[43] C. Weeraman, A. K. Yatawara, A. N. Bordenyuk, and A. V. Benderskii, "Effect of nanoscale geometry on molecular conformation: Vibrational sum-frequency generation of alkanethiols on gold nanoparticles," *J. Amer. Chem. Soc.*, vol. 128, no. 44, pp. 14244–14245, Nov. 2006.
[44] C. Humbert, B. Busson, J. P. Abid, C. Six, H. H. Girault, and A. Tadjeddine, "Self-assembled organic monolayers on gold nanoparticles: A study by sum-frequency generation combined with UV–vis spectroscopy," *Electrochimica Acta*, vol. 50, no. 15, pp. 3101–3110, May 2005.
[45] T. Kawai, D. J. Neivandt, and P. B. Davies, "Sum frequency generation on surfactant-coated gold nanoparticles," *J. Amer. Chem. Soc.*, vol. 122, no. 48, pp. 12031–12032, Dec. 2000.
[46] E. F. Takin *et al.*, "Barium titanate core–gold shell nanoparticles for hyperthermia treatments," *Int. J. Nanomed.*, vol. 8, pp. 2319–2331, Jun. 2013.
[47] J. Hao, J. Wang, X. Liu, W. J. Padilla, L. Zhou, and M. Qiu, "High performance optical absorber based on a plasmonic metamaterial," *Appl. Phys. Lett.*, vol. 96, no. 25, p. 251104, Jun. 2010.
[48] K. K. Du *et al.*, "Wavelength and Thermal Distribution Selectable Microbolometers Based on Metamaterial Absorbers," *IEEE Photonics J.*, vol. 7, no. 3, pp. 1–8, Jun. 2015.
[49] A. Moreau *et al.*, "Controlled-reflectance surfaces with film-coupled colloidal nanoantennas," *Nature*, vol. 492, no. 7427, pp. 86–89, Dec. 2012.
[50] J. B. Lassiter *et al.*, "Third-harmonic generation enhancement by film-coupled plasmonic stripe resonators," *ACS Photon.*, vol. 1, no. 11, pp. 1212–1217, Nov. 2014.
[51] L. Kang, Y. Cui, S. Lan, S. P. Rodrigues, M. L. Brongersma, and W. Cai, "Electrifying photonic metamaterials for tunable nonlinear optics," *Nature Commun.*, vol. 5, no. 4680, Aug. 2014.
[52] R. W. Boyd, *Nonlinear Optics*. San Francisco, CA, USA: Academic, 2003.
[53] J. Liu *et al.*, "Generalization of the FDTD algorithm for simulations of hydrodynamic nonlinear drude model," *J. Comput. Phys.*, vol. 229, no. 17, pp. 5921–5932, Aug. 2010.
[54] P. Ginzburg, A. V. Krasavin, G. A. Wurtz, and A. V. Zayats, "Nonperturbative hydrodynamic model for multiple harmonics generation in metallic nanostructures," *ACS Photon.*, vol. 2, no. 1, pp. 8–13, Jan. 2015.
[55] M. Fang, Z. Huang, W. E. I. Sha, X. Y. Z. Xiong, and X. Wu, "Full hydrodynamic model of nonlinear electromagnetic response in metallic metamaterials," *Prog. Electromagn. Res.*, vol. 157, pp. 63–78, Oct. 2016.
[56] X. Y. Z. Xiong *et al.*, "Strongly enhanced and directionally tunable second-harmonic radiation by a plasmonic particle-in-cavity nanoantenna," *Phys. Rev. A*, vol. 94, no. 5, p. 053825, Nov. 2016.
[57] X. Y. Z. Xiong, L. J. Jiang, W. E. I. Sha, Y. H. Lo, and W. C. Chew, "Compact nonlinear Yagi-Uda nanoantennas," *Sci. Rep.*, vol. 6, Jan. 2016, Art. no. 18872.